MATERIALS PHYSICS AND MECHANICS RESEARCH ARTICLE

Submitted: March 9, 2026 **Revised: April 2, 2026** **Accepted: April 29, 2026**

Stochasticity of dynamic straining and high-velocity ejection of particles under shock loading

Yu.I. Meshcheryakov [1], A.K. Divakov [1], A.L. Gaikov [2], G.V. Konovalov ✉[1], N.I. Zhigacheva [1]

[1] Institute for Problems of Mechanical Engineering RAS, St. Petersburg, Russia

[2] St. Petersburg Institute of Technology (Technical University), St. Petersburg, Russia

✉ goldenten@yandex.ru

ABSTRACT

Shock-tests of 1565 aluminum alloy under uniaxial strain conditions show that within local regions of target of 100–200 μm a significant increase in mass velocity occurs. Microstructural investigations of specimens revealed a presence of traces of local deformation in the form of narrow shear bands directed perpendicular to the free surface of the target. Simultaneously an ejection of particles from the back side of the target occurs. The discovered phenomenon correlates with the stochastic character of mesostructure behavior at the mesoscopic scale level. Theoretically, the stochasticity of shock-wave propagation in shock deformed solids is taken into account by using the mesoparticle velocity distribution function which is incorporated into the Klein-Gordon equation. The solution to this equation shows that shock-wave amplitude is determined by the relationship between viscosity and velocity variation of mesostructure.

KEYWORDS

mesoparticle • stochasticity • ejection • scale • alloy • impact • shock-wave

Funding. *The work has been performed in the frame of State Assignment of Ministry of Science and High Education of Russian Federation for Institute of the Mechanical Engineering Problems IPMash RAS (No 124041500007-4).*

Citation: Meshcheryakov YuI, Divakov AK, Gaikov AL, Konovalov GV, Zhigacheva NI. Stochasticity of dynamic straining and high-velocity ejection of particles under shock loading. *Materials Physics and Mechanics*. 2026;54(3): 42–53.
http://dx.doi.org/10.18149/MPM.5432026_4

Introduction

The high-velocity ejection of particles during the shock-wave loading attracts an attention of specialists in dynamic deformation and fracture. This process is speculated to be related to the action of high-velocity jets on initiating the Meshkov-Richtmaier instability in the explosive nuclear problem [1]. To date different mechanisms of shock-induced ejection are considered in physics and mechanics of shock-wave processes. Specifically, in [2,3], the numerical methods for the calculation of ejection are developed. They have observed the ejection of copper elements from grain boundaries at the free surface. Such ejection is also reported in [4]. Macroscopic models of high-velocity ejection suppose that the dimensions of ejected particles are determined by the shock-wave front configuration [5]. It should be noted that the known macroscopic models of ejection do not account for the stochastic character of the motion of the elementary carriers of deformation [6,7]. By the way, it has been shown that velocity distribution, i.e., stochasticity, presents else at the dislocation scale level [8,9]. The dislocation velocity dispersion, D^2, was found to be inversely proportional to dislocation viscous drag, B, of the medium:

© Yu.I. Meshcheryakov, A.K. Divakov, A.L. Gaikov, G.V. Konovalov, N.I. Zhigacheva, 2026.
Publisher: Peter the Great St. Petersburg Polytechnic University
This is an open access article under the CC BY-NC 4.0 license (https://creativecommons.org/li-censes/by-nc/4.0/)

$$D^2 = \frac{1}{(2\pi)^3}\frac{b^4}{B^2}\mu\rho, \quad (1)$$

where b is the Burgers-vector, μ is the shear modulus, ρ is the material density.

In the present paper, an investigation of the influence of stochasticity of dynamic straining on the high-velocity ejection of particles under shock loading is carried out at the mesoscopic scale level. This investigation includes the following stages.

1. Experimental investigation of shock-wave processes in heterogeneous media at two scale levels - mesoscopic and macroscopic levels.
2. Formation of mesostructure and nucleation of stochasticity of dynamic straining under shock loading.
3. Modeling the shock-wave propagation in a heterogeneous medium with accounting for the stochasticity.
4. Microstructural investigation of post-shocked specimens.

Shock tests

Within the frame of the first direction, a series of shock tests of 1565 aluminum alloy targets has been carried out. Response of material on shock loading was registered with the developed interferometric technique (for further - interferometer IPME RAN) which allows to register the stochastic characteristics of shock-wave process on two scale levels - variation of mass velocity (square root of the particle velocity dispersion) at the mesoscale-1 (5–10 μm) and loss of the shock-wave amplitude, ΔU, (velocity defect) at the macroscopic scale level as a difference between impact velocity under symmetrical collision and free surface velocity of target [10]. Owing to fine focusing of interferometer beam the wave profile corresponds to the dynamic behavior of a single structural element of meso-2 scale (50–100 μm). The velocity distribution of meso-1 particles within the limits of the single meso-2 particle is characterized by the velocity variation D_{ms1}. Difference between impact velocity and maximum mass velocity at the shock pulse plateau determines a loss of shock wave amplitude $\Delta U = U_{imp} - U_{fs\,max}$, which is the so-called velocity defect. In Fig. 1, the time dependencies of the free surface velocity, U_{fs}, and velocity variation, D_{ms1}, are presented.

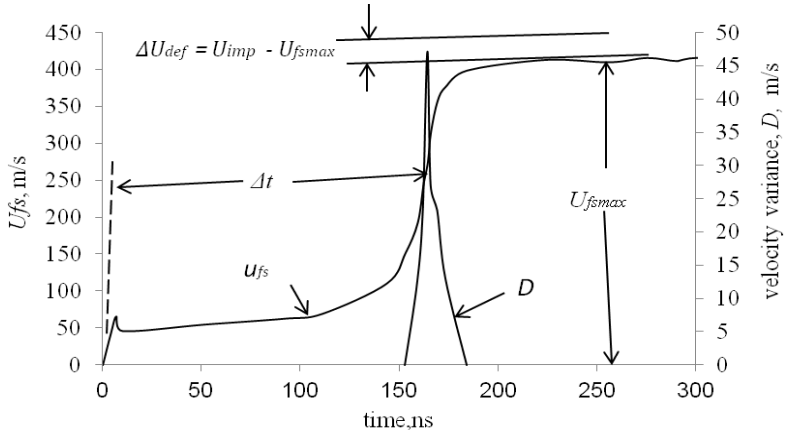


Fig. 1. The time profiles of the free surface velocity, U_{fs}, and velocity variation, D, in aluminum alloy target loaded at the impact velocity of 428 m/s

In Fig. 2, on the basis of a series of analogous dependencies registered for the shock lading with different impact velocities, the dependencies for velocity variation D_{ms-1} and the velocity defect ΔU as a function of impact velocity are presented. It may be concluded:
1. Velocity variation at the mesoscale-1 is increased from zero value at the impact velocity of 242 m/s up to D_{ms-1} = 52.2 m/s at the impact velocity of 450 m/s. Velocity variation is constant within the impact velocity range of 450–523 m/s. At the impact velocity of 523 m/s velocity variation begins to decrease up to zero at the impact velocity of 625.5 m/s.
2. Velocity defect changes weakly within the impact velocity range of 242–523 m/s. However, beginning from the velocity of 523 m/s it begins to decrease. At the impact velocity of 625.5 m/s it falls up to - 14.4 m/s.

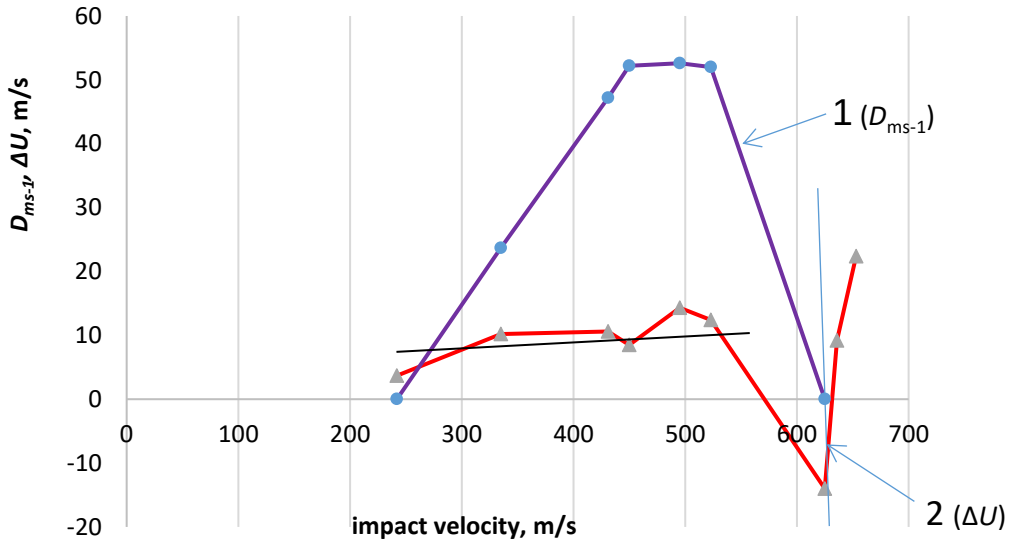


Fig. 2. Dependencies of velocity variation, D_{ms-1} (1) and velocity defect, ΔU (2) on the impact velocity

Analysis of the dependencies testifies to the presence of correlation in their of behavior. Within impact velocity range of 523–625.5 m/s when the velocity variation mesoscale-1 decrease, the velocity defect decreases as well. The zero value of the velocity variation means that elementary carriers of deformation begin to move at the same velocities. At the same time, the fact that the velocity defect becomes negative, means that instead of decreasing, the free surface velocity increases. Such a kind of behavior of the velocity defect is found for the first time.

Formation of mesoparticle and stochasticity under shock loading

The most important specifics of dynamic deformation of solids are the time correlations among elementary carriers of deformation [11–14]. The collective processes lead to the formation of structural elements the space scale of which is much more than the dislocation scale. In this situation, for the adequate description of deformation processes, the so-called mesoscopic scale level of deformation has been introduced [15–20]. In accordance with [20], the basic distinctive feature of mesoscale is that under the action of stress fields the rebuilding of initially an uniform quasi-neutral distribution of dislocations into non-uniform distribution is initiated - most of the dislocations are

separated in sign and accumulated in narrow layers, i.e., heterogenisation of dislocation ensemble occurs.

The above mechanism of mesostructure formation is proper to quasistatic strain rates. The mesostructure formation in an ensemble of moving dislocations flows on a different manner. For understanding and describing the mechanisms of formation of dynamic mesostructure, two important factors must be taken into account: (a) interaction of dislocations with the medium where they move, (b) interaction of dislocations with each other. In Fig. 3, a series of dependencies for the relative density of single-sign dislocations in A-95 aluminum is presented for dislocation drag viscosity of $B = 10^{-3}$ ps.

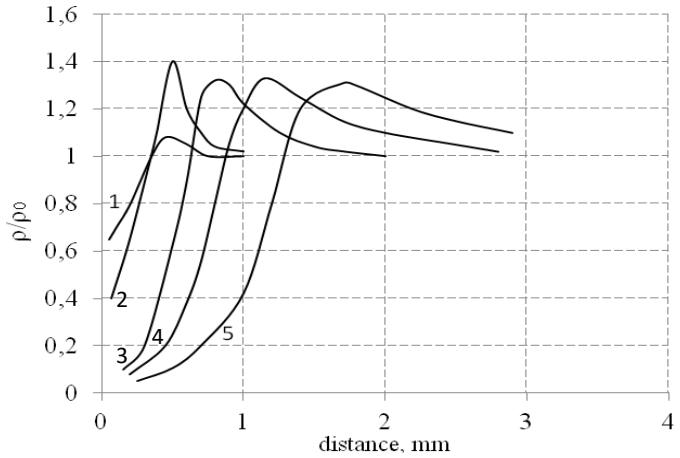


Fig. 3. Space profiles of relative density of dislocations for $B = 10^{-5}$ ps for different time moments: 1 — 45 ns, 2 — 60 ns, 3 — 90 ns, 4 — 120 ns, 5 — 150 ns

The time moment $t = 45$ ns corresponds to the beginning of mesostructure formation when the grouping of single-sign dislocation is else not developed so the dislocation structure remains chaotic. To the moment of $t = 60$ ns the relative density of single-sign dislocations reaches a maximum value of $\frac{\rho}{\rho_0} = 1.4$. After that the mesostructure is gradually blurred, so that at the moment of $t = 150$ ns the dislocations are again uniformly distributed. Formation of dynamic mesostructure occurs for 40–60 ns. For that time, the single-sign dislocations are localized within space region of 500 nm after which a uniform chaotization of the dislocation ensemble occurs.

The short-time grouping of dislocations and following transition back into chaotic distribution can present the pulsations of mass velocity which results in the generation of stochasticity of dynamic deformation. In physical kinetics the quantitative characteristic of the chaotic mass pulsations is known to be the velocity distribution function. In other words, the shock-induced stochasticity of dynamic deformation is generated at the stage of mesostructure formation.

Incorporation of stochasticity into shock-wave propagation

The mathematical approach developed for uniformly distributed dislocations is thought to be applicable to the meso-structure with the distinction that the Burgers-vector for each mesoparticle herein equals to sum of all the Burgers-vectors of dislocations constituting the mesoparticle [21]. The additional step in modeling the shock-wave

propagation in solids is incorporating the concept of physical kinetics for mesostructure. The physical kinetics of mesostructure deals with the mesoparticles velocity distribution function. This allows the shock-wave propagation in solids to consider with the accounting for the stochasticity of dynamic deformation process. The concept of physical kinetics for mesostructure has been introduced in [9]. In accordance with that concept, the mesostructure is the chaotically distributed single-sign dislocation groups. The mesosparticle velocity distribution function for this field is the second rank tensor the components of which $f_{ik}(r,v,t)$ characterize the combination of mesoparticles of different the Burgers-vectors and of differently directed of dislocation groups. Taking into account the tensor feature of the mesoparticle velocity distribution function, the statistical moment of the order *m* in the velocity space is the second rank tensor (*m*+*2*):

$$M_m = \int_{-\infty}^{\infty} \vec{v}\ldots\vec{v} f_{ik} d\vec{v}, \quad (2)$$

where $\vec{v}\ldots\vec{v}$ is the tensor of rank m. The zero statistical moment of the mesoparticle velocity distribution function determines the mean density of single-sign dislocations, i.e. the mean density of mesoparticles:

$$\rho_{ik}(r,t) = \int_{-\infty}^{\infty} f_{ik}\,(\vec{r},\vec{v},t) d\vec{v}. \quad (3)$$

The first statistical moment determines the flow tensor of mesoparticles:

$$j_{ij}(\vec{r},t) = e_{ikl} \int_{-\infty}^{\infty} v_l f_{kj}\,(\vec{r},\vec{v},t) d\vec{v}, \quad (4)$$

whereρ_{ik} is the *ik* component of the density tensor of mesoparticles, J_{ij} is the components of the flow tensor for mesoparticles, *r* is a coordinate, v is a mass velocity, *m* is the mass of the mesoparticle, *t* is time.

The statistical moments of the mesoparticle velocity distribution function coincide with the analogous characteristics for continuum dislocation theory. The distinctive specifics of the kinetic theory of mesostructure is a presence of the item responsible for the interaction of mesoparticles with the medium. This feature follows from the presence of additional items in the equation for mesoparticle motion. In this equation, besides the Peach-Koehler force $F = \sigma b$ the item Bu is presented. This item characterizes the viscous drag of mesoparticles [22–25]:

$$m\frac{\partial u}{\partial t} = \sigma b - Bu, \quad (5)$$

where *b* is the Burgers-vector, *B* is a drag coefficient of mesostructure. In one-dimensional situation the kinetic equation looks as follows [9]:

$$\frac{\partial f}{\partial t} + u\frac{\partial f}{\partial x} + \left(\frac{F}{m} + \frac{B}{m}u\right)\frac{\partial f}{\partial u} + \frac{B}{m}f = H_{col}, \quad (6)$$

where H_{col} is the so-called collision item of the kinetic equation for mesostructure. As distinct from physical kinetics of gas and liquid, where the particles interact only with each other, the convective part of the kinetic equation for mesostructure, due to the dependence of the acceleration of mesoparticles on the velocity of mesoparticles, contains additional items:

$$\frac{B}{m}u, \frac{B}{m}f. \quad (7)$$

In this section, the main task is the application of the physical kinetic approach to the determination of shock-wave amplitude in a heterogeneous medium with accounting for the stochastic features of the dynamic deformation process. In order to take into account for the stochastic features of mesostructure the continuum theory of moving dislocations adopted to the mesostructure of single-sign dislocations is used [26–28].

$$\rho\frac{\partial u}{\partial t}=\frac{\partial \sigma}{\partial x},$$
$$\frac{\partial u}{\partial x}=\frac{\partial \varepsilon}{\partial t}+J,\sigma=(\lambda+2\mu)\varepsilon, \quad (8)$$
$$J(x,v)=b\int_{-\infty}^{\infty}vf(x,v)dv.$$

Here σ is a normal stress, ε is a deformation, u is the mean mesoparticle velocity, $J(x,v)$ is the mesoparticle flow tensor, *f(x,v)* is the mesoparticle velocity distribution function. In order to account for the stochasticity, the tensor flow $f(x,v)$ is expressed via mesoparticle velocity distribution function. Equations (8) can be presented in the form of two rank differential equations:

$$\rho\frac{\partial^2 u}{\partial t^2}-(\lambda+2\mu)\frac{\partial^2 u}{\partial x^2}+\rho\frac{\partial J}{\partial x}=0. \quad (9)$$

The mesoparticle velocity distribution function in Eq. (9) can be presented in the form equilibrium and non-equilibrium parts:

$$f=f_0+f_1,\ f_1<<f_0. \quad (10)$$

Equilibrium mesoparticle velocity distribution function looks as following [29]:

$$f_0(x,v)=\left(\frac{B}{\pi F_2 m}\right)^{\frac{1}{2}}\rho(x)\,exp\left[-\frac{B}{F_2 m}(v-u)^2\right]. \quad (11)$$

In turn, the non-equilibrium part may be expressed via a relaxing form of the kinetic equation [30]:

$$\frac{\partial f_1}{\partial t}+u\frac{\partial f_1}{\partial x}+\langle\dot{u}\rangle\frac{\partial f_1}{\partial u}=-\frac{f-f_0}{\tau}, \quad (12)$$

where τ is the relaxation time for the mesoparticle velocity distribution function. Because of the small value of relaxation time, the change of the mesoparticle velocity distribution function due to relaxation processes occurs much more quickly than due to convective mass transportation. Therefore, the first two items in Eq. (12) can be neglected. Then:

$$f_1=-\frac{\sigma b}{m\tau}\frac{\partial f_0}{\partial u}, \quad (13)$$

and Eq. (9) takes the form:

$$\frac{\partial^2 u}{\partial x^2}-\frac{1}{C_l^2}\frac{\partial^2 u}{\partial t^2}+\frac{\partial u}{\partial x}\left\{-\frac{2B}{m}\xi\tau\sqrt{\frac{\pi}{\xi}}\int_{-\infty}^{\infty}v(v-u)\left(\frac{\sigma b}{B}-u\right)exp\left[-\frac{B}{F_2 m}(v-u)^2\right]\right\}dv=0, \quad (14)$$

where

$$\xi=\frac{B}{Dm}. \quad (15)$$

The value $v_p=\frac{\sigma b}{B}$ is the mean mesoparticle velocity. Exchanging $u(x,t)=g(x,t)e^{\frac{Ax}{2}}$ yields:

$$u_{tt}=g_{tt}e^{\frac{Ax}{2}},u_x=g_x e^{\frac{Ax}{2}}+ge^{\frac{Az}{2}}\cdot\frac{A}{2},u_{xx}=g_{xx}e^{\frac{Ax}{2}}+Ag_x e^{\frac{Ax}{2}}+ge^{\frac{Ax}{2}}\frac{A^2}{4}, \quad (16)$$

where

$$A=\frac{8\rho}{\sqrt{2}}\left(1-\frac{\tau B}{m}\right). \quad (17)$$

In turn, substitution into Eq. (14) yields:

$$\frac{1}{C_0^2}\frac{\partial^2 u}{\partial t^2}-\frac{\partial^2 u}{\partial x^2}+A\frac{\partial u}{\partial x}=0. \quad (18)$$

This is the well-known Klein-Gordon equation. One should substitute the following boundary and initial conditions:

$$\begin{Bmatrix}u(0,t)=u_0(t)\\ \frac{\partial u}{\partial x}(L,t)=0\end{Bmatrix}, \quad (19)$$

$$\left\{\begin{matrix} u(x,0)=\eta_1(x) \\ u(x,0)=\eta_2(x) \end{matrix}\right\} \left\{\begin{matrix} u(0,t)=u_0(t) \\ \frac{\partial u}{\partial x}(L,t)=0 \end{matrix}\right\}, \quad (20)$$

$$g(x,t)=C_0^2\frac{\partial^2 g}{\partial x^2}-G^2 g, \quad (21)$$

where

$$G=\frac{b(\lambda+2\mu)}{2\sqrt{2}}\left(1-\frac{\tau B}{m}\right)=A\frac{(\lambda+2\mu)}{2\rho}=C_0^2\frac{A}{2}, \quad (22)$$

The boundary conditions for Eq. (21) look as following:

$$\left\{\begin{matrix} u(0,t)=u_0(t) \\ \frac{\partial u}{\partial x}(L,t)=0 \end{matrix}\right\}, \quad (23)$$

$$g(x,0)=\left[exp(-\frac{Ax}{2})\right]f_1(x), \frac{\partial g}{\partial t}(x,0)=\left[exp(-\frac{Ax}{2})\right]f_2(x). \quad (24)$$

Solution to Eqs. (18)–(24) is searched in the form:

$$g(x,t)=\omega(x,t)+v(x,t), v(x,t)=u_0(t). \quad (25)$$

For variable $\omega(x,t)$ the non-uniform Klein-Gordon equation with zero initial conditions is obtained. Here:

$$F(x,t)=-G^2u_0(t)-\frac{\partial^2 u_0}{\partial t^2}, \quad (26)$$

$$\omega(0,t)=0, \frac{\partial\omega}{\partial x}(L,t)=0, \quad (27)$$

$$\omega(x,0)=f_1(x)-u_0(0), \omega_t(x,0)=f_2(x)-u_0(0). \quad (28)$$

Solution to Eqs. (26)–(28) can be found in the form:

$$\omega(x,t)=\sum_{n=0}^{\infty}T_n(t)X_n(x), \quad (29)$$

$$F(x,t)=\sum_{n=0}^{\infty}F_n(t)X_n(x), F_n(t)=\frac{2}{L}\int_0^L Fx,t)\,X_n(x)dx, \quad (30)$$

$$X_n(x)=sin\left(\frac{\pi(2n+1)}{2L}x\right)=sin(k_nx), \quad (31)$$

where $X_n(x)$ are the own functions of Sturm-Liuville task:

$$X''+k^2X=0,\ X(0)=0,\ X'(L)=0, \quad (32)$$

and $\lambda_n=k_n^2=\left[\frac{\pi(2n+1)}{2L}\right]^2$ are own values.

Substitution Eq. (30) into (26) yields:

$$T_n''(t)+\omega_n^2T_n(t)=F(t), \quad (33)$$

$$\omega_n^2=C_0^2\lambda_n+G^2. \quad (34)$$

The solution to Eq. (33) is:

$$T_n(t)=A_n(t)\,cos(\omega_nt+B\,sin(\omega_nt)+\frac{1}{\omega_n}\int_0^t F_n(s)\,sin[\omega_n(t-s)]\,ds, \quad (35)$$

$$A_n=\frac{2}{L}\int_0^L\omega(x,0)X_n(x)dx,\ B_n=\frac{2}{\omega_nL}\int_0^L\frac{\partial\omega}{\partial t}(x,0)X(x)dx. \quad (36)$$

In case of loading with the rectangular pulse:

$$u_0(t)=u_0[\Theta(t)-\Theta(t-t_0)], \quad (37)$$

where

$$\Theta(t)=1, t\geq 0,$$
$$\Theta(t)=0, t<0, \Theta(t)=1, t\geq 0, \quad (38)$$
$$\Theta(t)=0, t<0.$$

$$F_n(t)=-\frac{4}{\pi(2n+1)}\left[G^2u_0(t)+\frac{\partial^2u_0(t)}{\partial t^2}\right]. \quad (39)$$

When $f_1(x)=f_2(x)\equiv 0, A_n=B_n=0$:

$$T_n(t)=\frac{1}{\omega_n}\int_0^t F_n(s)\,sin[\omega_n(t-s)]\,ds=-\frac{4u_0}{\pi(2n+1)\omega_n}\Psi. \quad (40)$$

$$\Psi=\int_0^t G^2[\theta(s)-\theta(s-t)]+\left[\delta'(s)-\delta'(s-t)\right]sin[\omega_n(t-s)]\,ds. \quad (41)$$

We use the relationship:

$$\int f(x)\delta^n(x)dx = (-1)^n \int f^{(n)}(x)\,dx. \quad (42)$$

Then,

$$\Psi = \frac{G^2-\omega_n^2}{\omega_n}[cos(\omega_n(t-t_0) - cos(\omega_n t)] = 2\frac{G^2-\omega_n^2}{\omega_n} sin\frac{\omega_n t_0}{2} sin\left[\omega_n(t-\frac{t_0}{2})\right]. \quad (43)$$

As a result, one obtains:

$$T_n(t) = \frac{8u_0}{\pi(2n+1)}\frac{\omega_n^2-G^2}{\omega_n^2} sin\frac{\omega_n t_0}{2} sin\left[\omega_n(t-\frac{t_0}{2})\right]. \quad (44)$$

Then the amplitude of shock wave becomes:

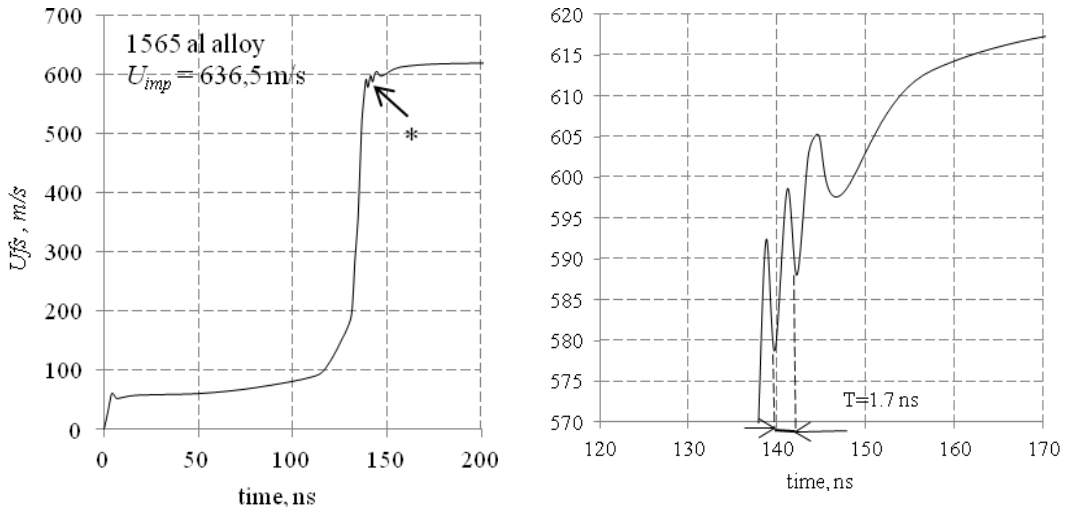
$$u(x,t) = e^{\frac{Ax}{2}}[u_0(t)] + \sum_{n=0}^{\infty}\frac{8u_0}{\pi(2n+1)}\frac{\omega_n^2-G^2}{\omega_n^2} sin(\frac{\omega_n t_0}{2}) sin\left[\omega_n(t-\frac{t_0}{2})\right] sin\left[\frac{\pi(2n+1)}{2L}x\right]. \quad (45)$$

The specific feature of obtained solution is that the bracket $(1-\frac{\tau B}{m})$ which switches the regime of shock-wave propagation is presented both in amplitude coefficients of Eq. (45) in the form of $exp(\frac{Ax}{2})$, and in the argument:

$$G = C_0^2(\frac{Ax}{2}),\ \omega_n^2 = C_0^2\lambda_n + G^2. \quad (46)$$

Consider the meaning of bracket $(1-\frac{\tau B}{m})$. In accordance with Eq. (1), when the viscous decay *B* increases the velocity variation decreases. The sign of the bracket $(1-\frac{\tau B}{m})$ depends on the value of drag coefficient *B*. The negative sign of bracket leads to change the sign before first derivative in Eq. (10) which leads to non-equilibrium regime of shock-wave propagation. Besides, in accordance with Eqs. (45) and (46), this simultaneously leads to narrowing of the shock-wave front. In other words, the bracket $(1-\frac{\tau B}{m})$ determines not only the value of the velocity defect ΔU, but also regulates of its width - the greater amplitude of the velocity defect, the much narrow becomes the time profile.

The question arises, what is the reason for velocity synchronization for the elementary carriers of deformation of mesoscale-1. The synchronization results from the oscillations of plastic wave straining at the shock wave [31–33]. In the case of 1565 aluminum alloy, the oscillations are seen under impact velocity of 625.5 and 636.5 m/s. The time period of 1.7 ns corresponds to the space period of L = 9.6·10^{-4} cm, i.e., meso scale-1 level. In Fig. 4, as example, the oscillations at the impact velocity of 636.5 m/s are presented.



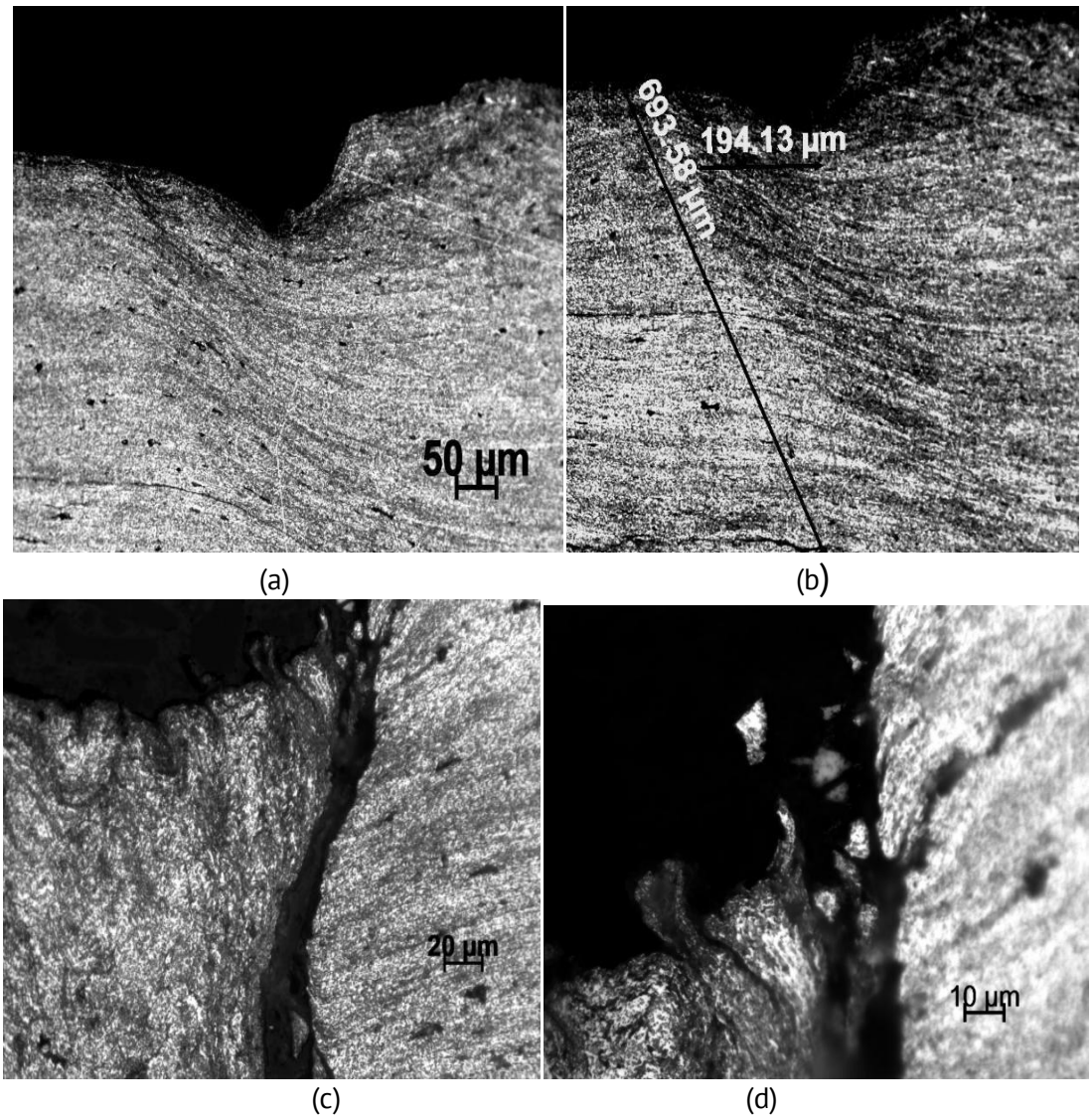
(a) (b)

Fig.4. Oscillation of plastic wave at the impact velocity of 636.5 m/s. Period of oscillation is 1.7 ns

In 1565 aluminum alloy under impact velocities of 625.5 and 636.5 m/s the elementary carriers of deformation of mesoscale-1 (1–10 μm) come into resonance with the shock-wave front which leads to synchronization of their velocities. The synchronization occurs within dimensions of the single element of mesoscale-2 so this is a local event. Thus, the initiation localized flow of medium occurs in the following scenario: (1) resonance interaction of shock-wave with the elementary carriers of deformation of mesoscale-1 and (2) synchronization of collective motion of mesoscale-1 particles.

Microstructural investigations

Microstructural investigations were carried out on 1565 aluminum alloy targets loaded at the impact velocity of 625.5 m/s. After shock loading, all the specimens were cut along one of planes parallel to direction of shock, poisoned in Nitric acid and were investigated in Axio-Observer -Z-1m microscope. The basic attention was directed to the region near the free surface of the target. The traces of localized deformation were found only in 1565 aluminum alloy targets loaded at the impact velocity of 625.5 m/s. In Fig. 5,



(a) (b)

(c) (d)

Fig. 5. Localized traces in form of cracks caused by the ejection of particles

the valley of 200 μm in width is presented. The valley is oriented perpendicular to the free surface of the target. One can see also the traces of particle ejection the particles of 5–7 μm in size (Fig. 5(c,d)). Often the ejection of particles occurs from the cracks.

Conclusions

The investigation of high-velocity ejection under shock loading of plane 1565 aluminum alloy targets includes the following stages:
1. Shock tests under uniaxial strain conditions. The conditions for initiating the negative velocity defect were found when in local regions of mesoscopic scale (70–100 μm) the velocity of the free surface target is higher than the impact velocity. The negative velocity defect appears when the velocity variation of mesoscale-1 becomes equal to zero, i.e., all the carriers of deformation of mesoscale-1 move with identical velocities.
2. Procedure of formation of mesoparticle as a group of identical single-sign dislocations. In A95 aluminum the mesoparticle as a group of identical single-sign dislocations is found for 45 ns after what gradually changing for 50–700 ns. Herewith, the mesoparticle is considered to be a super-dislocation, the Burgers-vector of which equals sum of single-sign dislocations. The procedure of formation of mesoparticles is thought to be a driving force for the stochasticity generation during the dynamic deformation process.
3. Solution to the Klein-Gordon equation shows that the amplitude of shock wave and the duration of the shock front are determined by the relationship between the velocity variation and the viscous drag of mesoparticles.
4. The microstructural investigations of post-shocked specimens reveals a presence of ejection from the back side of target and the traces of local deformation in the form of shear bands of 200 μm in diameter.
5. The valuable result of the investigation is thought to be the theoretical and experimental determination of conditions at which instead of decay a local mass acceleration in discrete regions of deformed body occurs.
6. This result causes the criteria for defending apparatus from cosmic debris to be reconsidered.

CRediT authorship contribution statement

Yuri I. Meshcheryakov: problem statement; derivation of the Klein-Gordon equation, writing – review & editing; **Alexander K. Divakov**: investigation; **Andrey L. Gaikov**: solving the shock wave propagation problem; **Grigory V. Konovalov**: investigation; **Natalia I. Zhigacheva**: microstructural investigation.

Conflict of interest

The authors declare that they have no conflict of interest.

References

1. Nellis WJ, Dlott D. Town Hall Meeting: Future Directions in Dynamic High Pressure Research. *AIP Conference Proceedings.* 2007;955(1): 12–16.

2. Yano K, Horie Y-Y. Discrete element modeling of shock compression of polycrystalline copper. *Physical Review B*. 1999;59(21): 13672–13680.
3. Baer MR. Computational modeling of heterogeneous reactive materials at the mesoscale. *AIP Conference Proceedings.* 2000;505(1): 27–34.
4. Remiot C, Chapron P, Demay B. A flash X-ray radiography diagnostic for studying surface phenomena under shock loading. *AIP Conference Proceedings.* 1994;309(1): 1763–1766.
5. Georgievskaya AB, Raevskii VA. Influence of shock-wave profile on distribution of dimensions of particles removed from the free surface of metals under shock loading. In: *XVII Kharitonov Readings: theses of reports.* Sarov: RFYaTs; 2015. p.340–341. (In Russian)
6. Horie Y, Kittel D, Sakano M. How plane are plane shock waves in solids. *AIP Advances*. 2023;13(6): 060701.
7. Horie Y. Three pearls of high-pressure shock compression of solids. *Journal of Dynamic Behavior of Materials.* 2024;10: 353–362.
8. Alekseev AA, Strunin BM. Viscous motion of dislocations in random fields of internal stresses. In: *Dislocation Dynamics*. Kiev: Naukova Dumka; 1975. p.132–137. (In Russian)
9. Meshcheryakov YuI, Prokuratova EI. Kinetic theory of continuously distributed dislocations. *International Journal of Solids and Structures*. 1995;32(12): 1711–1726.
10. Meshcheryakov YuI, Divakov AK. Multiscale kinetics of microstructure and strain-rate dependence of materials. *DYMAT Journal*. 1994;1(4): 271–278. (In Russian)
11. Efremov DV, Oborin VA, Uvarov SV, Naimark OB. Critical dynamics of localized instabilities of plastic flow in AMg6 alloy. *PNRPU Mechanics Bulletin*. 2017;4: 28–39.
12. Naimark O, Uvarov S, Bannikova I, Efremov D. Multiscale plastic shear instability as mechanism of turbulence. *AIP Conference Proceedings*. 2018;2051(1): 020209.
13. Uvarov S, Efremov D. Critical phenomena in Portevin-Le Chatelier effect during compression of aluminium-magnesium alloy and stored energy evolution. *Procedia Structural Integrity*. 2019;18: 309–313.
14. Efremov DV, Uvarov SV, Spivak LV, Naimark OB. Statistical laws of localization development of deformation under plastic flow in AMg6 alloy. *Letters on Materials*. 2020;10(1): 38–42.
15. Kanel GI, Ivanov MF, Parshikov AN. Computer simulation of the heterogeneous materials response to the impact loading. *International Journal of Impact Engineering*. 1995;17(1–3): 455–464.
16. Panin VE. Physical mechanisms of mesomechanics of plastic deformation and fracture of solids. *Acta Metallurgica Sinica.* 1997;33(2): 187–197.
17. Panin VE, Egorushkin VE, Panin AV. Physical mesomechanics of deformed solid as multilevel system. Physical basis for multilevel approach. *Physical Mesomechanics.* 2006;9(3): 9–22.
18. Makarov PV. On the hierarchic nature of deformation and fracture of solids. *Physical Mesomechanics.* 2004;7(4): 25–34.
19. Makarov PV. Physical mesomechanics approach in simulation of deformation and fracture processes. *Physical Mesomechanics.* 1998;1: 57–75.
20. Vladimirov VI, Nikolaev VN, Priemskii NM. Mesoscopic scale level of deformation. In: Zhurkov SI. (Ed) *Physics of Strength and Plasticity*. Leningrad: Nauka; 1986. p.69. (In Russian)
21. Gutkin MYu, Ovid'ko IA, Meshcheryakov YuI. Mechanisms of rotational effect in shock-loaded crystalline metallic materials. *Journal de Physique III France.* 1993;3(8): 1563–1579.
22. Meshcheryakov YuI. Statistical description of dislocation structure on the basis of Fokker-Planck equation. *Numerical Techniques of Mechanics of Continuum Medium.* Novosibirsk; 1974;5(3): 157–162. (In Russian)
23. Kumar A, Hauser FE, Dorn JE. Viscous drag on dislocations in aluminum at high strain rates. *Acta Metallurgica*. 1968;16(9): 1189–1197.
24. Predvoditelev AA. Modeling of the processes related to motion and multiplication of dislocations in crystals. In: *Dislocation Dynamics*. Kiev: Naukova Dumka; 1975. p.178–195. (In Russian)
25. Al'shits VI, Idenbom LV. Dynamic drag of dislocations. In: *Dislocation Dynamics*. Kiev: Naukova Dumka; 1975. p.232–275. (In Russian)
26. Kosevich AM. *Dislocations in Elastic Theory*. Moscow: Nauka; 1978. (In Russian)
27. Mura T. Continuous distribution of moving dislocations. *Philosophical Magazine*. 1963;8(89): 843–857.
28. Head AK, Wood WW. Dislocation group dynamics IV. General solutions of the continuum approximation. *Philosophical Magazine*. 1973;27(3): 505–517.
29. Meshcheryakov Yu. *Multiscale Mechanics of Shock Wave Processes*. Singapore: Springer; 2022.

30. Kihara N, Aono O. Unified Theory of Relaxations in Plasmas, I. Basic Theorem. *Journal of the Physical Society of Japan*. 1963;18(6): 837–851.
31. Meshcheryakov YuI, Divakov AK, Zhigacheva NI, Konovalov GV, Osokin EP. Comparative analysis 1: incipient stage of dynamic deformation and fracture in 1561 and 1565 aluminum alloys. *Problems of Strength and Plasticity*. 2022;84(3): 409–419.
32. Meshcheryakov YuI, Konovalov GV, Divakov AK, Zhigacheva NI, Osokin EP. Investigation of multiscale mechanisms of dynamic deformation and fracture of 1565 aluminum alloy under plane collision and high-velocity penetration. *Materials Physics and Mechanics*. 2020;46(1): 70–87.
33. Meshcheryakov YuI, Divakov AK, Zhigacheva NI, Konovalov GV, Barakhtin BK, Kalinin GYu, Fomina OV. Dynamic strength of nitrogen steel. *Materials Physics and Mechanics*. 2014;21(2): 99–111.